JMEPEG (1992) 1:91-96

Comparison of Corrosion-Fatigue Properties of 6013 Bare, Alclad 2024, and 2024 Bare Aluminum Alloy Sheet Materials

J. Chaudhuri, Y.M. Tan, K. Patni, and A. Eftekhari

A corrosion-fatigue test was performed on Alclad 2024, 2024 bare, and 6013 bare aluminum alloy sheet materials to compare their respective corrosion-fatigue resistance. In addition, metallographic and scanning electron fractographic examinations of some of the tested specimens were performed to evaluate the mode of cracking and the nature of failure in these materials. It was found that Alclad 2024 had superior resistance to corrosion compared to the 2024 bare and 6013 bare specimens, with the 2024 bare performing slightly better than the 6013. Fractographic and microstructural examinations showed that the clad layer of Alclad 2024 provided protection to its base metal from corrosion, resulting in longer corrosion-fatigue life. The lower corrosion-fatigue life of the 6013 bare material was due to intergranular corrosion.

1 Introduction

THE 6013 alloy (Al-0.8Si-0.9Cu-0.95Mg-0.35Mn) sheet material is finding increasing usage in new aircraft designs due to the following beneficial properties.

1. Good stretch-forming characteristics in T4 temper (solution heat treated and naturally aged to a substantially stable condition), comparable to that in the 2024 (Al-4.4Cu-0.6Mn-1.5Mg) in W temper (solution heat treated, applicable only to alloys that spontaneously age at room temperature). This property helps in reducing fabrication costs.
2. Finer grain size than conventional aluminum sheet materials such as the 2024 alloy. The fine grain size helps to minimize orange peel condition during stretch-forming operations.
3. Weldability comparable to that of the 6061 alloy.
4. The cost of the 6013-T6 sheet material comparable to that of the Alclad (cathodic protection to corrosion) 2024-T3 sheet material.
5. Higher tensile and compressive yield strengths when compared with Alclad 2024.
6. Three percent lower density than the 2024 alloy.
7. Fatigue and fracture toughness comparable to that of Alclad 2024.
8. 25 percent higher strength than the 6061 alloy sheet material.

The potential applications of this material include structural parts such as wing and fuselage skins, and fuselage bulkheads traditionally fabricated from Alclad 2024 and the 2024 bare sheet materials.

Earlier investigations on salt-spray corrosion resistance testing[1,2] concluded that the general corrosion in the 6013 alloy sheet material follows a narrow intergranular path. This characteristic is in contrast to that of 2024 alloy, which develops relatively wide corrosion pits. Hence, it was necessary to compare the corrosion-fatigue properties[3] of the 6013 bare sheet material with that of Alclad 2024 and 2024 bare sheet materials to realize the application of this material.

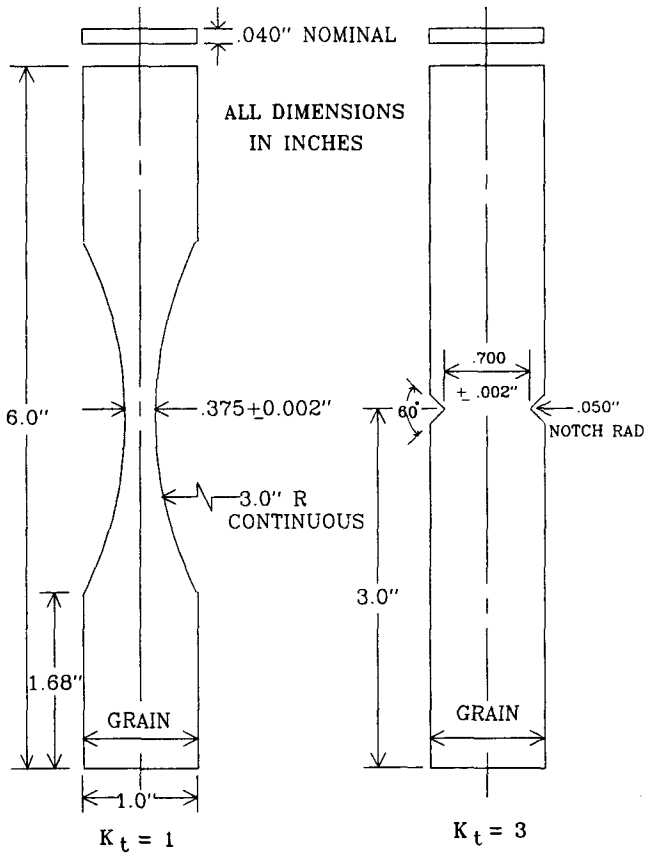

Fig. 1 Test specimen geometry.

J. Chaudhuri and **Y.M. Tan** are with the National Institute for Aviation Research, Mechanical Engineering Dept., The Wichita State University, Wichita, Kansas. **K. Patni** and **A. Eftekhari** are with Cessna Aircraft Company, Aircraft Division, Wichita, Kansas.

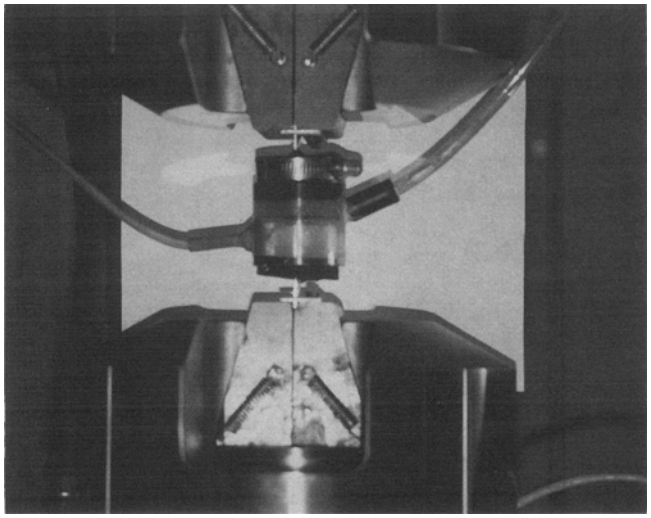

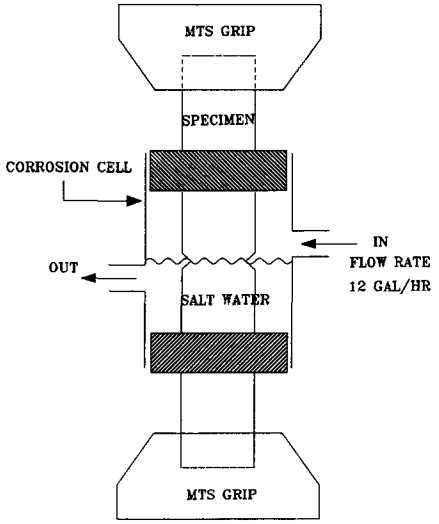

Fig. 2 Corrosion cell setup.

2 Experimental Conditions

Test specimens were fabricated from 0.040-in. thick 6013-T6, Alclad 2024-T3, and 2024-T3 bare sheet materials. The test specimen geometries were as shown in Fig. 1 for stress concentration factors $K_t = 1$ and $K_t = 3$, respectively. Tensile property tests of all materials were conducted per ASTM E108 to verify proper materials and heat treatments.

Constant-amplitude corrosion-fatigue tests were conducted at a frequency of 30 cycles per minute (*i.e.*, 0.5 Hertz). Maximum stress levels are listed in Table 1. The stress ratio between the maximum and minimum load of the fatigue cycling was 0.1 for all the test specimens. A corrosion cell was placed around the test specimen gage area (Fig. 2). A uniform and linear flow of 3.5% aerated salt water was maintained through the corrosion cell at 10 to 12 gallons per hour flow rate (Fig. 2).

3 Results

3.1 *Corrosion-Fatigue Test Results*

Corrosion-fatigue test data are shown in Table 2. The fatigue cycling of Alclad 2024-T3 specimens was terminated after 200,000 cycles. It was observed that at 20 ksi and $K_t = 1$, the Alclad 2024-T3 alloy has more than 5.8 times longer corrosion-fatigue life than the 6013-T6 alloy and more than 2.5 times longer corrosion-fatigue life than the 2024-T3 bare sheet material (Fig. 3). At 15 ksi and $K_t = 3$, the Alclad 2024-T3 alloy has a 2.6 times longer fatigue life than the 6013-T6 alloy and 1.9 times longer fatigue life than the 2024-T3 bare alloy (Fig. 4). In addition, the fatigue data for the 6013-T6 bare alloy showed more scatter at 15 ksi and $K_t = 3$ as compared to that of Alclad 2024-T3 and 2024-T3 bare alloys (Table 2 and Fig. 4).

Table 1 Test Specimen Matrix

Test specimen	Maximum stress, ksi	Stress concentration factor, K_t	No. of repeats
2A20K1	20	1	3
2A15K3	15	3	3
3A20K1	20	1	3
3A15K3	15	3	3
6A20K1	20	1	3
6A15K3	15	3	6
6A10K3	10	3	3

Note: Total number of specimens = 24.2A20K1 is Alclad 2024-T3 specimen. 3A20K1 is 2024-T3 bare specimen. 6A20K1 is 6013-T6 bare specimen.

3.2 *Visual Examination*

All fatigue-cycled specimens were visually examined for the extent of surface decolorization to determine the surface corrosion adjacent to the fracture surface. Of the three groups of materials tested, the Alclad 2024 specimens showed the least amount of corrosion and 2024 bare specimens showed the maximum. The 6013 specimens had surface corrosion in between Alclad 2024 and 2024 bare specimens.

3.3 *Fractographic Examination*

Scanning electron microscopic (SEM) examination was conducted on a notched specimen from each group of materials. These specimens were 2A15K3-2 (Alclad 2024), 3A15K3-2 (2024 bare), and 6A15K3-2 (6013). Each of these specimens had the lowest fatigue life in its own group.

The Alclad 2024 specimen exhibited a relatively smooth fracture surface and had only one primary crack origin site at the notch. No corrosion damage was observed adjacent to the crack

Table 2 Corrosion-Fatigue Test Results

Sample No.	Stress, ksi	Stress corrosion factor, K_t	Thickness, in.	Width, in.	Force applied	Cycles to failure	Average No. of cycles
2A20K1-1	20	1	0.0400	0.375	300	>241000	
2A20K1-2	20	1	0.0390	0.375	293	>202141	>200000
2A20K1-3	20	1	0.0400	0.375	300	...	
3A20K1-1	20	1	0.0400	0.375	300	94151	
3A20K1-2	20	1	0.0400	0.375	300	81495	80564
3A20K1-3	20	1	0.0400	0.376	301	66047	
6A20K1-1	20	1	0.0400	0.375	300	33701	
6A20K1-2	20	1	0.0390	0.375	293	24863	34151
6A20K1-3	20	1	0.0390	0.375	293	43889	
2A15K3-1	15	3	0.0400	0.699	419	139560	
2A15K3-2	15	3	0.0390	0.698	408	106728	118345
2A15K3-3	15	3	0.0390	0.699	409	108748	
3A15K3-1	15	3	0.0390	0.701	410	68048	
3A15K3-2	15	3	0.0390	0.700	410	50257	60753
3A15K3-3	15	3	0.0400	0.700	420	63954	
6A15K3-1	15	3	0.0400	0.700	420	82790	
6A15K3-2	15	3	0.0400	0.702	421	21875	
6A15K3-3	15	3	0.0400	0.698	419	53666	
6A15K3-4	15	3	0.0400	0.702	421	45793	45245
6A15K3-5	15	3	0.0400	0.703	422	28210	
6A15K3-6	15	3	0.0400	0.703	422	39135	
6A10K3-1	10	3	0.0400	0.698	279	103917	
6A10K3-2	10	3	0.0400	0.700	280	138699	121477
6A10K3-3	10	3	0.0400	0.702	281	121814	

Note: 2A20K1-1 designates Alclad 2024-T3 specimen No. 1 at 20 ksi stress and $K_t = 1$. 3A20K1-1 designates 2024-T3 bare specimen No. 1 at 20 ksi stress and $K_t = 1$. 6A20K1-1 designates 6013-T6 bare specimen No. 1 at 20 ksi stress and $K_t = 1$.

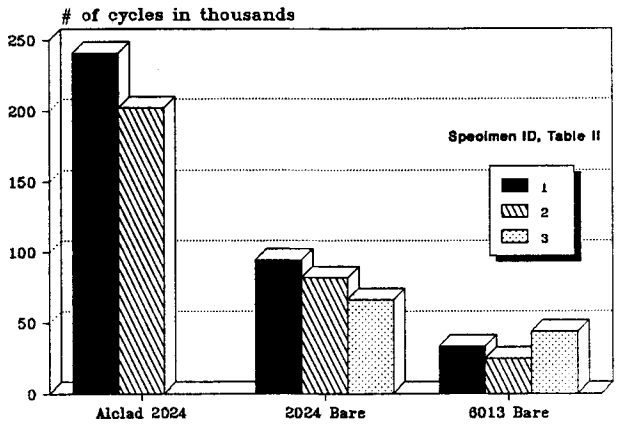

Fig. 3 Corrosion-fatigue life at 20 ksi and $K_t = 1$.

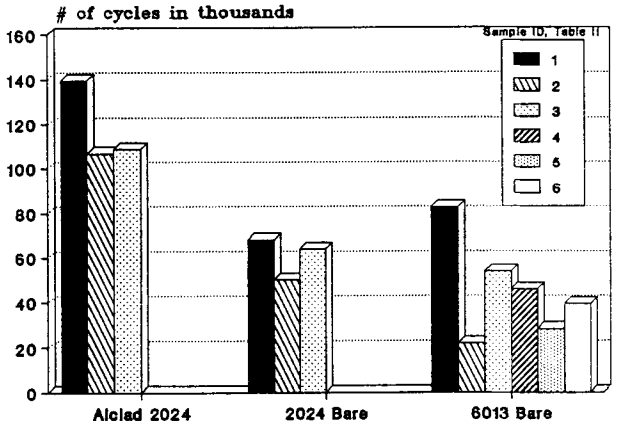

Fig. 4 Corrosion-fatigue life at 15 ksi and $K_t = 3$.

origin site (Fig. 5 through 7). The soft Alclad layer was primarily responsible for the fatigue initiation.

The 2024 bare specimen fracture surface had a rougher surface when compared to that of the Alclad 2024 and had multiple crack origin sites at the notch as well as at the specimen surface. It did not exhibit distinct steps. Corrosion pits were observed at the notch as well as on the specimen surface. Fatigue initiation was found to occur from these corrosion sites (Fig. 8 through 10).

The 6013 specimen fracture surface had three distinct steps resulting from the initiation and propagation of multiple cracks. The corrosion damage occurred mainly on the water inlet side almost along the whole width of the specimen. High magnification examination showed that the corrosion was intergranular. Figures 11 through 13 show the fracture surface features of the 6013 specimen.

3.4 *Metallographic Examination*

The microstructural examination using optical microscopy was conducted on the same specimens used for the fractographic

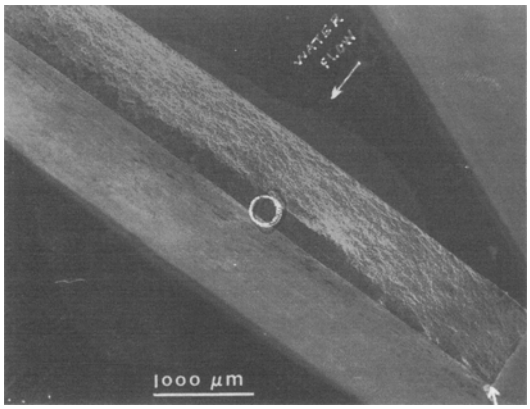

Fig. 5 Scanning electron macrograph of the Alclad 2024 fracture specimen indicating uniform fracture surface features and the crack origin site as marked by the arrow. See Fig. 6 for the enlarged view of the crack origin area and Fig. 7 for the enlarged view of the circled area. Magnification 20×.

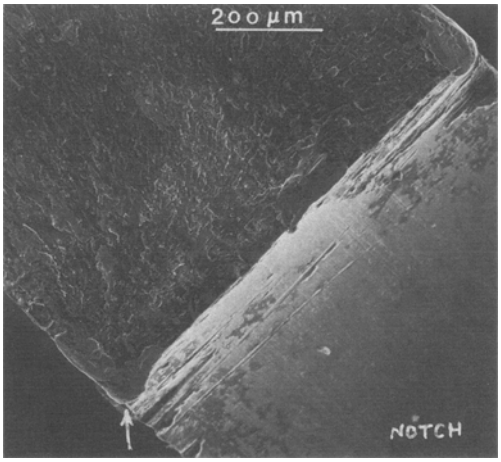

Fig. 6 Enlarged view of the crack origin area identified in Fig. 5 showing no indication of corrosion pitting (Alclad 2024). Magnification 100×.

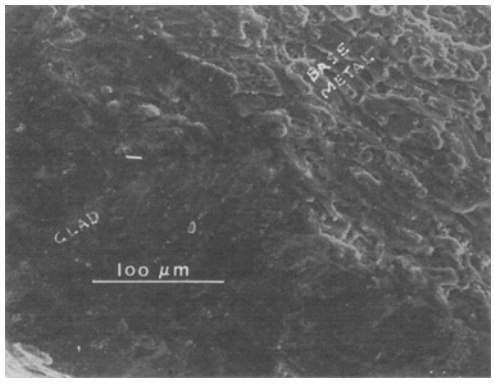

Fig. 7 Magnified view of the region inside the circle in Fig. 5. The base metal fracture surface did not show any evidence of damage by corrosion (Alclad 2024). Magnification 300×.

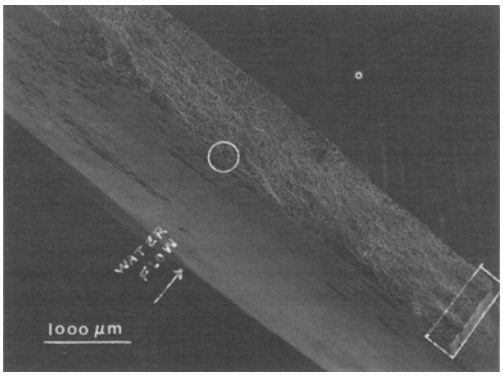

Fig. 8 Scanning electron macrograph of the 2024 bare fracture surface indicating multiple origin sites at the notch and on the specimen surface. Some crack origin sites were present at the opposite side of the notch also. See Fig. 9 for the enlarged view of the notch and the fracture surface adjacent to it marked by the rectangle. Also, see Fig. 10 for the enlarged view of the circled area. Magnification 20×.

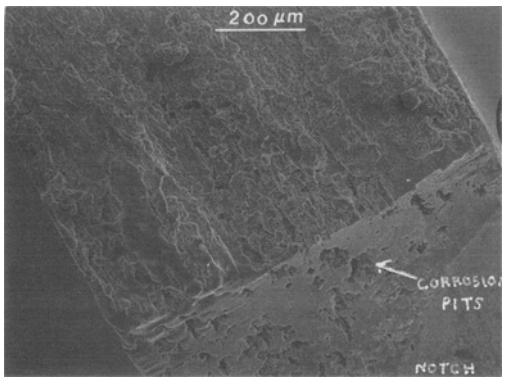

Fig. 9 Enlarged view of the region inside the rectangle shown in Fig. 8, indicating corrosion damage at the notch and on the fracture surface adjacent to the notch (2024 bare). Magnification 100×.

examination. The specimens were cross-sectioned at the location of maximum corrosion damage and metallurgical mounts were prepared. The microstructural examination showed that the corrosion did not penetrate completely through the cladding in the Alclad 2024 sample (Fig. 14). The 2024 bare sample had a number of transgranular corrosion pits on either side of the specimen thickness (Fig. 15). The depth of most severe corrosion pit in this sample was 0.007 in. The 6013 bare sample showed heavy intergranular corrosion damage to a depth of about 0.014 in. (Fig. 16). The heavy corrosion damage had occurred at the water inlet side of the specimen.

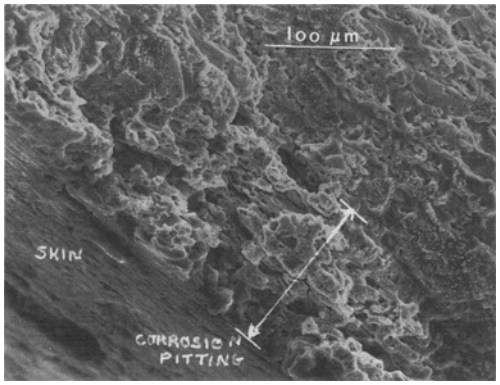

Fig. 10 Scanning electron micrograph of the region inside the circle in Fig. 8 showing corrosion pitting at the specimen surface (2024 bare). Magnification 300×.

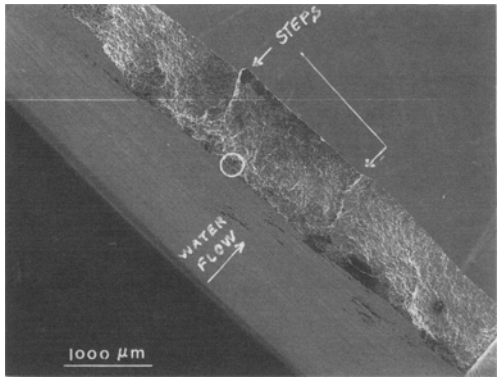

Fig. 11 Scanning electron macrograph of the 6013 bare fracture surface. The fracture surface exhibits steps, which indicate that the fracture occurred by the coalescence of the cracks initiated from multiple crack origin sites. See Fig. 12 for the enlarged view of the notch and Fig. 13 for the enlarged view of the circled area. Magnification 20×.

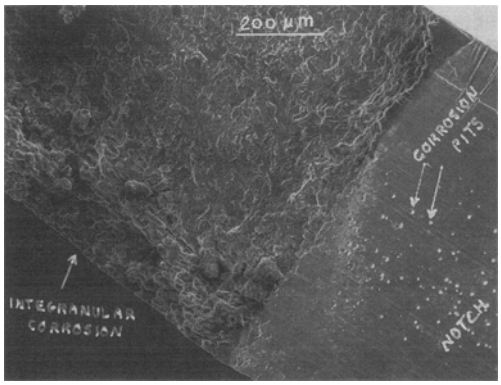

Fig. 12 Scanning electron micrograph of the fracture surface near the notch of the 6013 bare alloy showing corrosion pits at the notch. Magnification 100×.

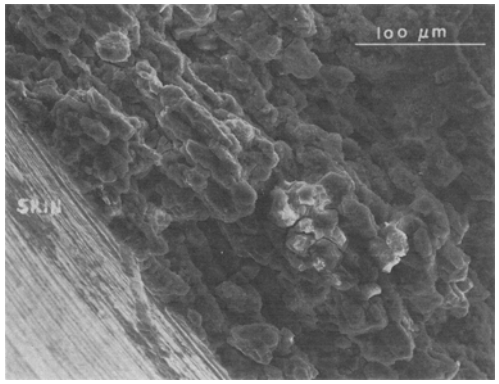

Fig. 13 Scanning electron micrograph of the region inside the circle in Fig. 11 showing intergranular corrosion adjacent to the specimen surface in the 6013 bare alloy.

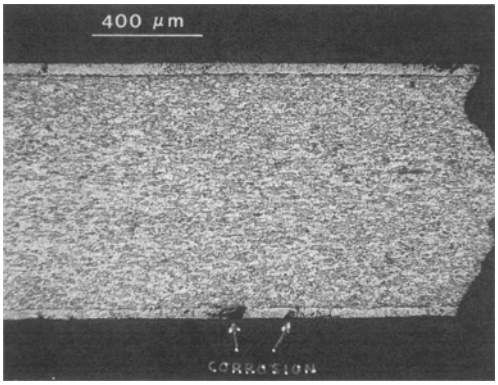

Fig. 14 Optical micrograph of the Alclad 2024 microsection showing no significant corrosion damage to the base metal. The microstructure also showed the grain size of the material finer than typically observed. Magnification 62.5×.

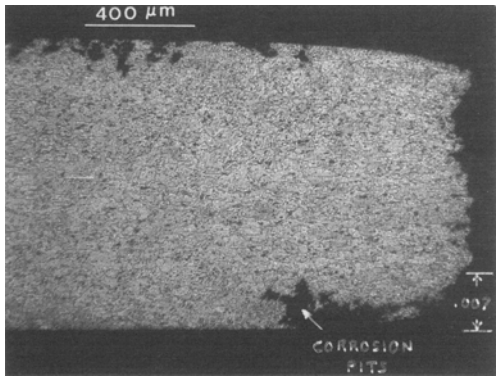

Fig. 15 Optical micrograph of the 2024 bare microsection showing large corrosion pits on both sides. It also showed the grain size of the material finer than typically observed. Magnification 62.5×.

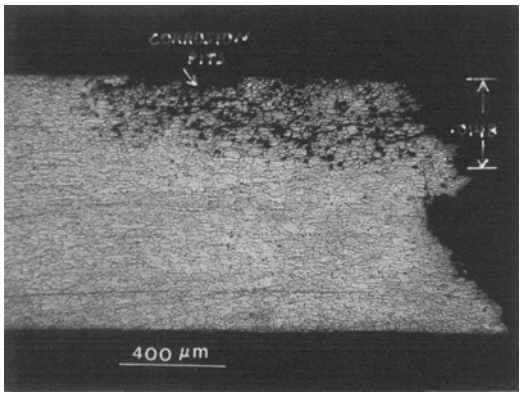

Fig. 16 Optical micrograph of the 6013 bare microsection showing corrosion pits and intergranular corrosion, which has penetrated about 30% of the specimen thickness. Magnification 62.5×.

4 Conclusion

The Alclad 2024-T3 material showed a much better corrosion-fatigue resistance compared to the 2024-T3 bare and 6013-T6 bare specimens. The 2024-T3 bare showed a slightly better corrosion-fatigue resistance than the 6013-T6.

Longer corrosion-fatigue life of the Alclad 2024-T3 was primarily attributed to the corrosion protection provided by the clad layer to the base metal. Lower life of the 6013-T6 bare was attributed to the observed intergranular corrosion.

Visual examination of the surface adjacent to the fracture surface indicated that the Alclad 2024 had the least amount of corrosion, 2024 bare the maximum, and 6013 in between.

Fractographic examination showed that the Alclad 2024 had a smooth fracture surface, with the crack originating from the notch. On the other hand, both the 2024 bare and 6013 bare had a rough fracture surface resulting from multiple crack initiations at the notch and at the surface of the specimens, particularly at the surface facing the water inlet. Moreover, the 6013-T6 bare fracture surface had distinct steps, indicating multiple crack propagations before coalescence to larger cracks.

Future work should be directed to compare the corrosion-fatigue resistance of the 6013 alloy with that of other aircraft skin materials, such as 7075 and 7475 aluminum alloys, and potential materials such as aluminum-lithium alloys. The effects of corrosion-preventive coatings and techniques should also be investigated to improve the corrosion resistance performance of all these materials. In addition, fatigue properties of precorroded 6013-T6 should be evaluated and compared with the corrosion fatigue data obtained in this study, because precorrosion is close to actual field conditions.

Acknowledgment

J. Chaudhuri and Y.M. Tan would like to acknowledge the grant from the Cessna Aircraft Co. and Kansas Technology Enterprise Commission.

References

1. J. Mavec, M & P Report No. 84-14-424, Cessna Aircraft Co., Wichita, May (1984).
2. K.M. Patni, M & P Report No. 90-87-017, Cessna Aircraft Co., Wichita, Apr (1990).
3. Corrosion Fatigue Failures, in *Metals Handbook*, vol. 9, 9th ed., ASM, Metals Park, OH, 252-262 (1985).